# The Effect of Organic and Metal Oxide Interfacial layers on the Performance of Inverted Organic Photovoltaics

*Achilleas Savva, Foteini Petraki, Polyvios Elefteriou, Lambrini Sygellou, Monika Voigt, Myrsini Giannouli, Stella Kennou, Jenny Nelson, Donal D. C. Bradley, Christoph J. Brabec, and Stelios A. Choulis**

**We study the origin of the improvement of the power conversion efficiency (PCE) of inverted organic solar cells when an interfacial insulating organic layer of polyoxyethylene tridecyl ether (PTE) is introduced between the indium tin oxide (ITO) bottom electrode and the $TiO_x$ interfacial layer. XPS and UPS measurements are used to investigate the energy level alignment at the interfaces within the ITO/$TiO_x$ and ITO/PTE/$TiO_x$ structures and to identify any effects due to chemical interaction and interfacial dipoles. Scanning electron microscopy studies show that the surface structure of the $TiO_x$ layer is affected, when it is coated on top of the PTE layer. Surface contact angle measurements show that the incorporated interfacial layer of PTE is more hydrophilic than ITO and thus PTE modified $TiO_x$ becomes more hydrophilic. This, in combination with the surface gaps of the PTE interfacial layer, is likely to lead to changed wetting and hydrolysis properties of $TiO_x$ when coated on ITO/PTE than on ITO alone. The different $TiO_x$ layer quality is reflected in improved electron selectivity, leading to enhanced fill factor, reduced parasitic resistance effects and higher power conversion efficiency for inverted solar cells with a PTE interfacial layer between ITO and $TiO_x$.**

## 1. Introduction

The world's demand for energy, combined with the inadequacy of fossil fuels to provide power for the rapidly rising human population, is motivation for the scientific community to search for "clean" renewable energy sources. Photovoltaics might be the most significant electricity source if the cost per kWh produced is further reduced. The cost reduction can either be achieved by lower cost of the current commercial solar cell technologies, or by the development of new solar cell materials and device concepts. Despite the lower power conversion efficiencies (PCEs), in comparison to other, conventional photovoltaic technologies,[1] organic photovoltaics (OPVs) have attracted a lot of attention, due to their high potential cost reduction for large area elements, their flexibility, light weight and transparency.[2,3] OPVs can offer many new applications for solar cells, ranging from self-powered electronics to energetically self-sufficient buildings.[4] At present, so-called bulk hetero-junction structures based on blends of a conjugated polymer as donor and a soluble fullerene derivative as acceptor represent the OPV material system with the highest power conversion efficiency reported until now. Recent developments include power conversion efficiencies up to 10%,[1] durability of 1 year under real environmental conditions,[5] accelerated lifetime test results indicating even longer OPV lifetimes[6] and proof of concept for high throughput fabrication using inkjet-printing and spray coating technologies.[7–11]

However, most of the published data are based on the "normal" bottom anode, top cathode device architecture. Most reported PCE values are higher for OPV devices in the normal architecture than in the "inverted" (bottom cathode, top anode) architecture using the same photoactive materials. Early attempts to make bulk hetero-junction organic solar cells with inverted polarity resulted in limited device performance due to carrier selectivity electrode issues.[12,13] Solution-processed $TiO_x$ on top of ITO gave improved charge selectivity and allowed the

A. Savva, P. Elefteriou, M. Giannouli, S. A. Choulis
Molecular Electronics and Photonics Research Unit
Department of Mechanical Engineering
and Materials Science and Engineering
Cyprus University of Technology
Limassol, 3603, Cyprus
E-mail: stelios.choulis@cut.ac.cy

F. Petraki, L. Sygellou, S. Kennou
Department of Chemical Engineering
University of Patras
Patra, 26504 Greece

DOI: 10.1002/aenm.201200317

M. Voigt, J. Nelson, D. D. C. Bradley
Department of Physics and Centre for Plastic Electronics
The Blackett Laboratory
Imperial College London
London SW7 2BZ, UK

C. J. Brabec
Institute for Materials in Electronics and Energy Technology
Friedrich-Alexander University Erlangen-Nuremberg
Erlangen, D-91058, Germany

C. J. Brabec
Bavarian Center for Applied Energy Research (ZAE Bayern)
Erlangen, D-91058, Germany

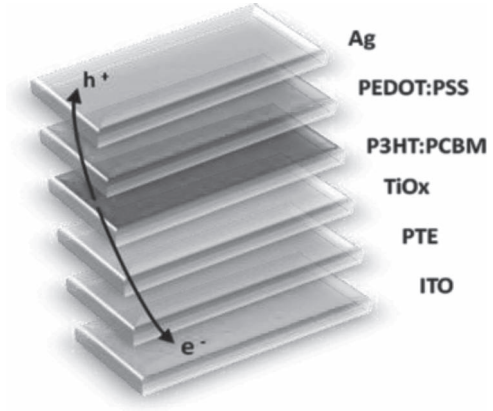


**Figure 1.** Device structure of the inverted solar cell using solution-processed organic (PTE) and metal oxide ($TiO_x$) interfacial layers as electron selective bottom contact.

processing of efficient inverted OPVs based on conventional active layer materials.[14] Other oxide based cathodes were used successfully in OPV devices.[15] Metal oxide-organic interfaces are important in controlling the charge extraction as well in controlling the three-dimensional phase structure. It is desirable to control the vertical segregation[16] of phases within the blend film, since this may assist in electrode selectivity and in directing the photocurrent.[17]

Inverted solar cells are attractive for large scale production of OPV devices because of compatibility with solution processing and this has stimulated more efforts to optimize inverted devices. Recently inverted devices have been reported with PCE values of 6–9% by using new active layer materials.[18–20] The prospect of all printed inverted cells has been assisted by the use of stamp transfer printed vapor phase polymerized PEDOT (VPP-PEDOT) as the top anode contact in inverted devices.[21]

We have reported that stacking of solution-processed organic and metal oxide interfacial layers gives highly charge selective, low resistance cathodes.[22] The structure of our inverted cells is ITO/PTE/$TiO_x$/P3HT:PCBM/PEDOT:PSS/Ag (**Figure 1**). The polyoxyethylene tridecyl ether (PTE) organic interfacial layer improved the electron extraction properties of the (ITO/$TiO_x$) bottom electrode.

In this paper, the interfaces formed, ex-situ, between ITO/PTE/$TiO_x$ are investigated by X-ray and ultraviolet photoelectron spectroscopy (XPS and UPS), scanning electron microscopy (SEM) and contact angle measurements. The aim of the XPS and UPS measurements was to investigate the existence of a chemical interaction between PTE and $TiO_x$ and possible changes in the cathode work function due to incorporation of PTE. SEM measurements were conducted in order to examine any differences in the surface of the $TiO_x$ layer when coated on top of PTE instead of ITO. Contact angle measurements were used to investigate the hydrophilicity of ITO and PTE layers and possible effects of the surface energy of PTE modified $TiO_x$ compared to ITO/$TiO_x$. Inverted organic solar cell devices with and without PTE interfacial layers were used to correlate the above investigations to solar cell device performance parameters.

## 2. Results and Discussion

The current density–voltage (J–V) characteristics of both sets of devices with and without PTE interfacial layer between ITO/$TiO_x$ were measured in the dark and under illumination at AM 1.5 G conditions and demonstrated in **Figure 2**a) and 2b) respectively. The External Quantum Efficiency measurements (EQE) for these devices are shown in Figure 2c). The results shown in Figure 2 are representative of our findings from testing over 50 similar devices.

The best device performance (PCE of 3.45%) was achieved with a combination of ITO/PTE/$TiO_x$ as electron selective contact. This represents an improvement of ~13% in performance relative to the best reference devices using ITO/$TiO_x$ as electron selective contact (PCE of 3.06%). As mentioned above, these results are consistent and reproducible and obtained from over 50 devices tested. The device performance was consistently higher when the PTE interfacial layer was introduced in the device, furthermore those observations are in agrement with our previous reported results.[22] From the dark J–V characteristics (Figure 2a), it is clear that the interfacial layer of PTE between ITO and $TiO_x$ reduces the leakage current (thus increasing the effective shunt resistance) and reduces the series resistance, which can be seen in the forward bias at +1 V as well. The reduced parasitic resistance effects can explain the higher fill factor (FF), and hence PCE, values found for the inverted cells using ITO/PTE/$TiO_x$ rather than ITO/$TiO_x$ as electron selective contact (Figure 2b). In illuminated J/V plots, both devices exhibit the same open circuit voltage ($V_{oc}$ = 0.58 V) which suggests that the recombination and morphology behavior are similar in the compared devices. The small increase in short circuit current density ($J_{sc}$) is due to reduced leakage current and reduced series resistance ($R_s$) observed for the diodes with ITO/PTE/$TiO_x$ electron selective contact.

Figure 2c) shows higher EQE values for ITO/PTE/$TiO_x$ in comparison with ITO/$TiO_x$ devices, which are in agreement with the J/V results shown above. The accuracy of the measurements has been confirmed by the calculation of the theoretical $J_{sc}$, which was calculated by multiplying the EQE by the AM1.5 G sun spectrum and integrating the result. The small mismatch factor (~4.43%) between the theoretical and experimental $J_{sc}$ indicates high accuracy measurements. A mismatch factor of 0.957 was determined. All PCE values reported in this paper have been calculated using a mismatch of 0.957.

X-ray photoelectron spectroscopy (XPS) (**Figure 3**) was used to investigate the chemical composition of the surfaces of the structures investigated and the effect of the PTE interfacial layer on the surface chemical structure.

The C1s XPS spectra, (Figure 3a), for ITO/$TiO_x$, ITO/PTE/$TiO_x$ and ITO reference structures are very similar with the main peak at a binding energy of 284.8 eV related to C−C, C−H, which originates from atmospheric contamination. In all cases the In, O and Sn peaks (not shown) from the ITO substrate were clearly observed. In the case of the ITO/PTE surface, the C1s XPS spectrum has a predominant peak at 286.8eV, mainly due to C−O−C and C−O−H bonds, indicating that this can be predominantly attributed to the PTE interfacial layer. The lower energy contribution is mainly attributed to the C−C and C−H bonds of PTE, as expected from the PTE chemical structure,

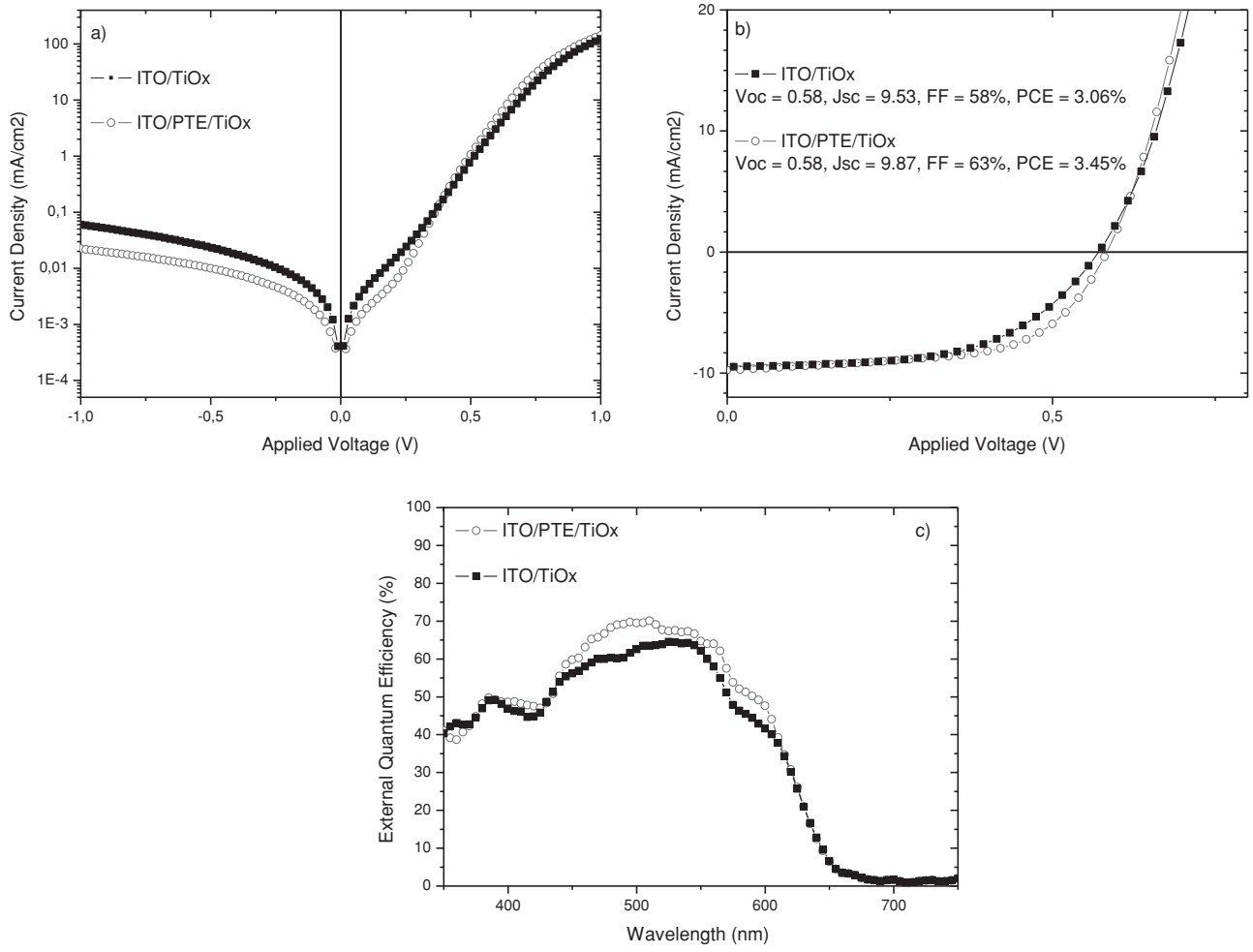


**Figure 2.** (a) Representative Dark current density-voltage characteristics of the solar cells under study. (b) Current density-voltage characteristics of the solar cells studied under illumination. (c) EQE measurements of the devices. All curves show J–V characteristics and quantum efficiencies for ITO/$TiO_x$ (square data points), and ITO/PTE/$TiO_x$ (circular data points) solar cell devices.

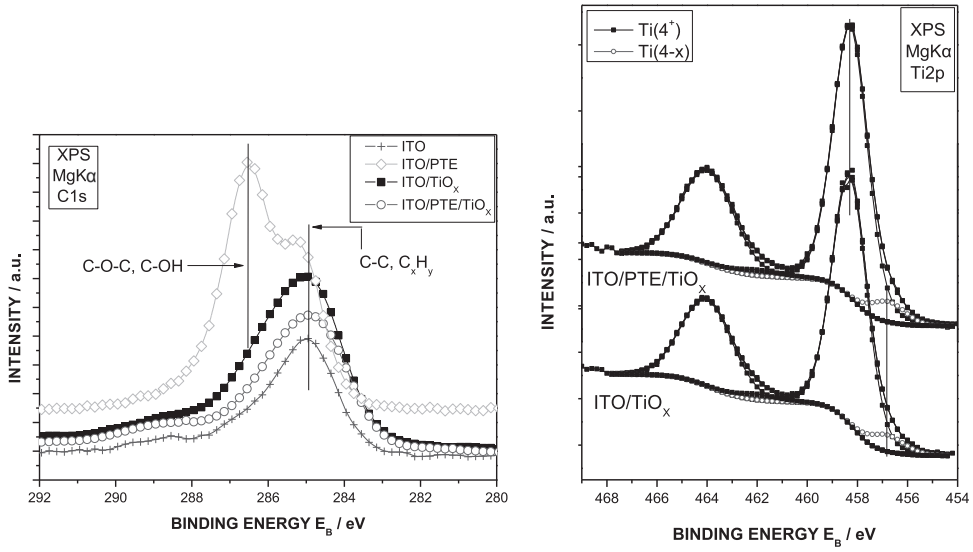


**Figure 3.** a) XPS spectra of C1s for ITO (data points are cross-shaped), ITO/$TiO_x$ (square data points), ITO/PTE (diamond-shaped data points) and ITO/PTE/$TiO_x$ (circular data points) interfaces. b) XPS spectra of Ti2p for ITO/$TiO_x$ and ITO/PTE/$TiO_x$ surfaces. Two types of curves are shown, one corresponding to the Ti(4+) oxidation state (square data points) and the other to the contribution from the lower oxidation states (circular data points).

suggesting that the contribution from atmospheric contamination is very small in this sample. PTE layer is best described as an interfacial layer, rather than a closed-layer (interlayer). Alternatively, the processing step with PTE can be considered as an interface conditioning step of ITO by PTE.

For both ITO/PTE/$TiO_x$ and ITO/$TIO_x$ interfaces, the Ti2p peak, (Figure 3b), appears at the same binding energy, where the main contribution is attributed to $TiO_2$. The Ti2p peak is deconvoluted in two Ti2p doublets: the higher binding energy (BE) component with the $Ti2p_{3/2}$ at 458.3 ± 0.1 eV corresponds to the Ti(4+) oxidation state, whereas the small, lower binding energy component with the $Ti2p_{3/2}$ at 456.8 ± 0.1 eV is assigned to a contribution of $Ti^{n+}$ states with n < 4. The Ti2p components are fitted with spin-orbit splitting of 5.7 eV for Ti(4+) and with spin-orbit splitting of 5.2 eV for the lower BE component, whereas the $2p_{3/2}$ to $2p_{1/2}$ ratio is 2:1.[23,24] The similarity of the spectra indicates that there is no chemical interaction between PTE and $TiO_x$.

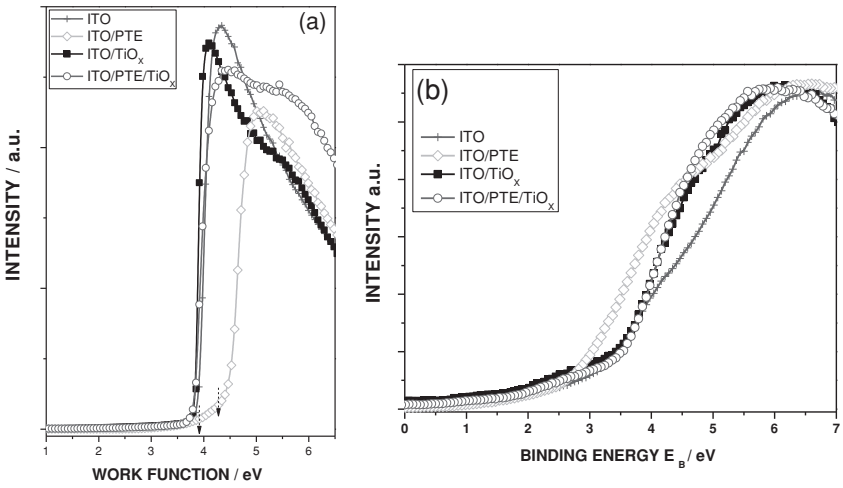


**Figure 4.** (a) Onset of the high binding energy cut-off of the UPS spectra and (b) valence band UPS spectra. The curves shown are for ITO (cross-shaped data points), ITO/$TiO_x$ (square data points), ITO/PTE (diamond-shaped data points) and ITO/PTE/$TiO_x$ (circular data points) samples.

Summarizing, we found no evidence of chemical interaction between PTE and $TiO_x$. The Ti peak is at the same binding energy for both structures (ITO/$TiO_x$ and ITO/PTE/$TiO_x$) corresponding predominantly to $TiO_2$ and shows no influence of the PTE layer presence, since the Ti2p is almost identical to the spectrum of structures without the PTE interfacial layer. Moreover, the fact that the XPS spectra of ITO/PTE/$TiO_x$ structures are dominated by features characteristic of $TiO_x$ indicates excellent coverage of the PTE by the $TiO_x$. The PTE should consequently not control the electron selectivity of the ITO/PTE/$TiO_x$/P3HT:PCBM/PEDOT:PSS/Ag device.

Next, the valence band structures and work functions of ITO/PTE/$TiO_x$, ITO/$TiO_x$ and ITO/PTE were investigated using ultraviolet photoelectron spectroscopy (UPS) (**Figure 4**). From Figure 4a it can be observed that the work function of ITO/$TiO_x$ is not significantly altered by the incorporation of the PTE interfacial layer. The work function, as derived from the High Binding Energy Cut-off (HBEC) value of the UPS spectra, of both electrodes under study is in the range of 3.9 eV ± 0.1 eV (onset of Figure 4a curves). The work function value measured for the as-received ITO surface is also in the same range. This value, both for contaminated ITO and $TiO_x$ surface, is in agreement with the literature[25] and is attributed to photochemical hydroxylation of the oxide surface induced by UV. This hydroxylation causes an oriented dipole on the surface, with the positively charged hydrogen atom directed outwards causing a reduction of the work function relative to the clean, unhydroxylated surface. The contamination hydrocarbon overlayer on the ITO substrate surface from the atmospheric exposure is also evidenced by the presence of the C1s XPS peak of the ITO curve in Figure 3a and it is estimated from the XPS measurements at about 1 nm.

The high binding energy cut-off spectrum of ITO/PTE, (Figure 4a), shows a clear shift in work function to 4.3 ± 0.1 eV. The interface dipole formation due to electron transfer from ITO to PTE leads to an increase of the work function and results in a vacuum level shift of 0.4 eV. This process takes place at the interface between the two materials. The valence band edge of PTE (Figure 4b) is found at 2.5 eV below the Fermi level and the calculated Ionization Energy (IE = $E_{HBEC}$ + HOMO), which is the value of the HOMO position from the vacuum level, equal to 6.8 eV. Figure 4b shows the presence of a tail of states at the ITO/PTE, ITO/$TiO_x$ and ITO/PTE/$TiO_x$ surfaces from 0.7 to 3.0 eV below the Fermi level. Such gap states may be attributed to oxygen deficiencies, as also deduced from the XPS spectra shown in Figure 3b). The ionization energy of $TiO_x$ on ITO was found to be equal to 7.1 ± 0.1 eV, very close to values reported in the literature.[25] This value was concluded from the (HBEC) work function value of 3.9 eV (obtained from the onset of Figure 4a curves), which represents the position of the vacuum level with respect to the Fermi level, and the HOMO position below the Fermi level at 3.0 eV (obtained from the onset of Figure 4b curves) for $TiO_x$, as previously.

It is interesting to construct the energy band line-up (**Figure 5**) for the ITO/PTE/$TiO_x$ (Figure 5a) and the ITO/$TiO_x$ interface (Figure 5b) taking into account the XPS and UPS experimental results. For the ITO substrate the valence band position was measured at 3.0 eV down from the Fermi level and taking from the literature the energy gap Eg = 3.6 eV,[25] the conduction band position can be drawn at 0.6 eV above the Fermi level. The work function value estimated at 3.9 eV determines the position of the vacuum level with respect to the Fermi level for the ITO substrate. For the ITO/PTE interface the position of the HOMO was found at 2.5 eV from the Fermi level and from the work function value at 4.3 eV, the vacuum level is drawn at 0.4 eV higher than the vacuum level position in the case of the ITO substrate. This 0.4 eV represents the dipole formation at the interface. When $TiO_x$ was deposited on PTE the valence band onset was found from the UPS data at 3.0 eV below the Fermi level and the $E_g$ was taken from the literature[24] equal to 3.3 eV, so the conduction band was at

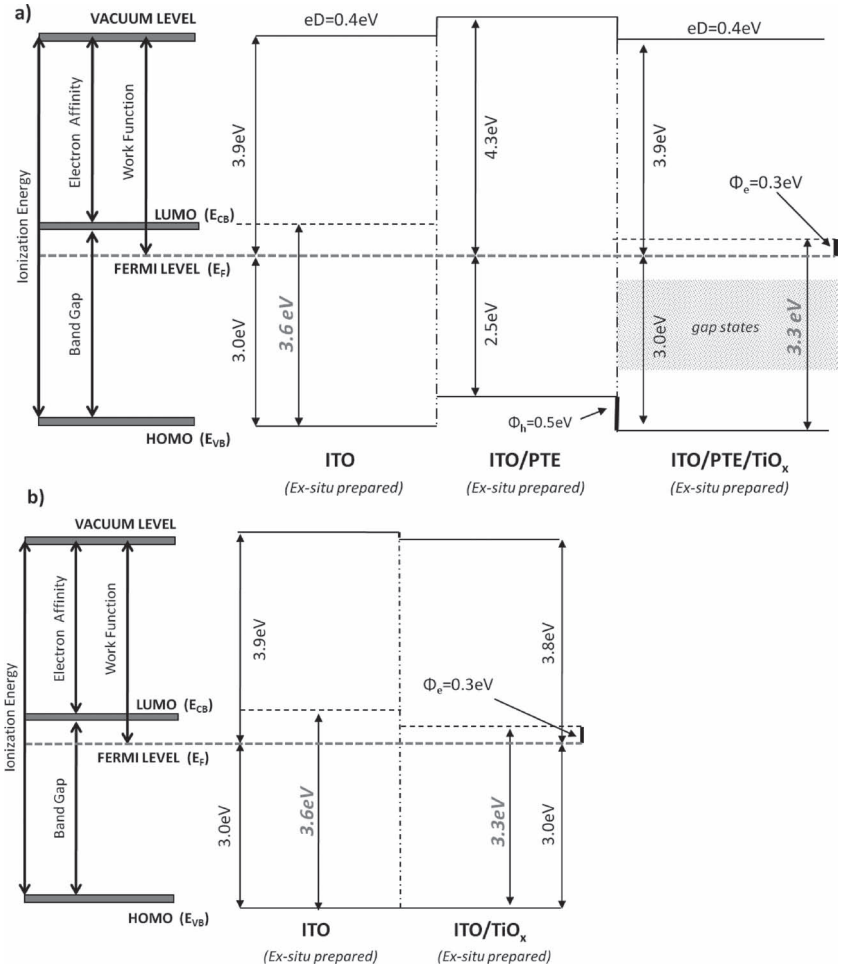


**Figure 5.** Schematic energy level diagram of the different investigated interfaces. a) ITO, ITO/PTE and ITO/PTE/$TiO_x$. b) ITO and ITO/$TiO_x$. The red-bold-italic values have been taken from the literature.[25–27]

0.3 eV above the Fermi level. The vacuum level is now located at 3.9 eV from the Fermi level as derived from the work function value. This gives a dipole downwards of 0.4 eV at the interface. In the ITO/PTE/$TiO_x$ structure, the hydroxylation of the $TiO_x$ surface generates dipoles in the opposite direction to the ITO/PTE interface dipole, resulting in a reduction of the work function and thereby facilitating electron injection.

From Figure 5a, for the ITO/PTE/$TiO_x$ structure, an offset of about 0.5 eV between the HOMO (highest occupied molecular orbital) of PTE and the valence band of $TiO_x$ is calculated, giving a hole injection barrier of 0.5 ± 0.2 eV. By considering the $TiO_x$ band gap to be 3.3 eV, the electron injection barrier is found to be 0.3 ± 0.1 eV. Such a small electron injection barrier is easily surmounted at room temperature. The aforementioned hole injection barrier is also very small and since the PTE layer is very thin, we expect hole transfer through tunneling to occur at the interface between the PTE and the $TiO_x$ surface. In the case of the ITO/$TiO_x$ interface (Figure 5b) the valence bands of ITO and $TiO_x$ are found to be aligned. A very small dipole formation was concluded from experimental measurements, of the order of the measurement accuracy (±0.1 eV). Also, the electron injection barrier was found to be the same (0.3 ± 0.1 eV), as for ITO/PTE/$TiO_x$. These results indicate that the presence of the interfacial PTE layer is unlikely to impact the internal potential difference across the active layer. The reported UPS measurements are in excellent agreement with our J-V measurements, showing that there is no difference in the built-in voltage ($V_{bi}$) for the devices using ITO/$TiO_x$ and ITO/PTE/$TiO_x$ as electron selective contact.[22] To summarize, the XPS and UPS studies indicate that there is no chemical interaction between PTE and $TiO_x$ altering the $TiO_x$ energy levels, nor is the electrode work function influenced by the PTE interface modification.

To further investigate the properties of ITO/PTE/$TiO_x$, bottom electrode high resolution SEM studies were performed. The aim of these studies is to investigate the influence of the PTE interface conditioning step on the surface of $TiO_x$.

**Figure 6**(a) and 6(b) shows that the PTE ultrathin layer is not a closed layer and it doesn't fully cover the ITO area. Surface gaps of different sizes are observed. When the $TiO_x$ layer is deposited on top of the PTE one, large clusters are formed (Figure 6d), which are not present in the ITO/$TiO_x$ film (Figure 6c). We believe that the clusters are formed due to PTE surface gaps in combination with the different wetting properties of the two materials. To validate this assumption we first tried to performed EDX analysis with SEM, at 1–30 keV but were not possible to reveal the composition of the clusters because the electronic beam penetrates the very thin interfacial layers (PTE below 10 nm and $TiO_x$~40 nm). Secondly, contact angle measurements were performed on the surface of each layer, as described in the experimental section.

Four different films relevant to the inverted OPV device structure (ITO, ITO/PTE, ITO/$TiO_x$ and ITO/PTE/$TiO_x$), were prepared with exactly the same process method used for our device structures. The contact angles of water, diiodomethane and ethylene glycol on top of each surface (ITO, ITO/PTE, ITO/$TiO_x$ and ITO/PTE/$TiO_x$) were measured. The water contact angles were found to be 89.5°, 67.1°, 102° and 94.3° respectively. This is an indication that the PTE surface is more hydrophilic than the ITO surface. To verify this hypothesis, the energy of each surface and the surface tension of the solutions of PTE (0.1% in water) and $TiO_x$ (precursor in Isopropanol) were measured. **Figure 7** shows the wetting envelopes of the surfaces and the surface tensions of the solutions. A short description of wetting envelopes and their function is given in the experimental section.

Due to the size of the wetting envelopes, it is clear that the PTE surface is more hydrophilic than the ITO surface. The increased hydrophylicity of the PTE layer is expected to improve

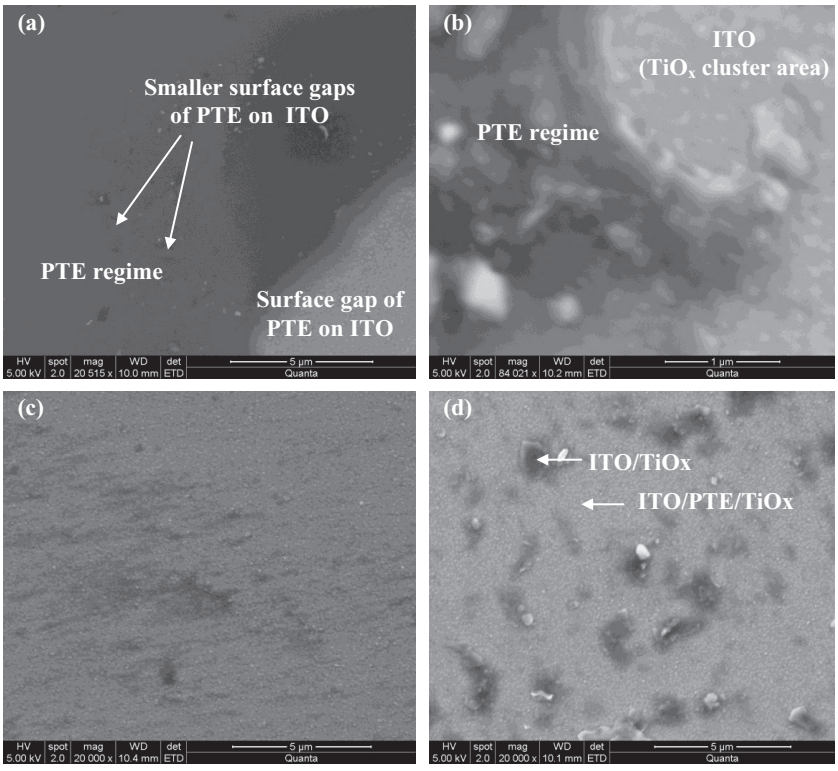


**Figure 6.** Scanning electron microscopy images of (a) ITO/PTE (b) ITO/PTE higher magnification (c) ITO/$TiO_x$ and (d) ITO/PTE/$TiO_x$.

the dispersion of the $TiO_x$ precursor solution. In addition, the surface tension of the PTE liquid is lying inside the wetting envelope of ITO. This means that homogeneous layers can be obtained. However, because PTE is an ultrathin interfacial layer, it is not a closed layer, surface gaps are observed (Figure 6a and 6b). More importantly, since PTE is an insulating material, a thicker and closed PTE interlayer between ITO and $TiO_x$ would have blocked electron collection. Furthermore, it can be observed that high quality layers of $TiO_x$ can be obtained on top of both ITO and PTE, because the surface tension of $TiO_x$ is lying well inside ITO and ITO/PTE wetting envelopes. We believe that the clusters of $TiO_x$ layers are formed due to a combination of the difference in hydrophilicity between ITO and PTE, and the surface gaps of the PTE interfacial layer. When the liquid precursor of $TiO_x$ is spread on the surface, it is forced by the more hydrophilic material (PTE) to move towards the less hydrophilic parts of the surface that are only covered with ITO. This results in the formation of clusters in the areas where there are gaps in the PTE layer and changes the surface of the ITO/PTE/$TiO_x$ layer (Figure 6d) compared to the ITO/$TiO_x$ layer (Figure 6c). This effect can be responsible for the reduced leakage current and $R_s$ observed in Figure 2b, by increasing the functionality of the layer and thus electron selectivity.

Furthermore, from wetting envelope calculations it was proved that $TiO_x$ becomes more hydrophilic when it is coated on top of PTE instead of ITO. The combination of the different morphology and hydrophilicity of $TiO_x$ could cause a different behavior of the active layer when coated on top of ITO/PTE/$TiO_x$ and ITO/$TiO_x$, similar to what we proved for $TiO_x$ when coated on top of ITO or PTE. Khodabakhsh et al. have shown that changes in surface wettability influence how the subsequently deposited organic molecules assemble and orient themselves, thus affecting the density of available charge collection sites in organic solar cells.[28] Enhanced vertical phase segregation occurred when the active layer was coated on top of more hydrophilic surfaces and there was higher accumulation of PCBM from the surface of increased hydrophilicity.[29] The enhanced vertical phase segregation can be responsible for the increased electrode selectivity in devices with PTE between ITO and $TiO_x$ as reported before.[17]

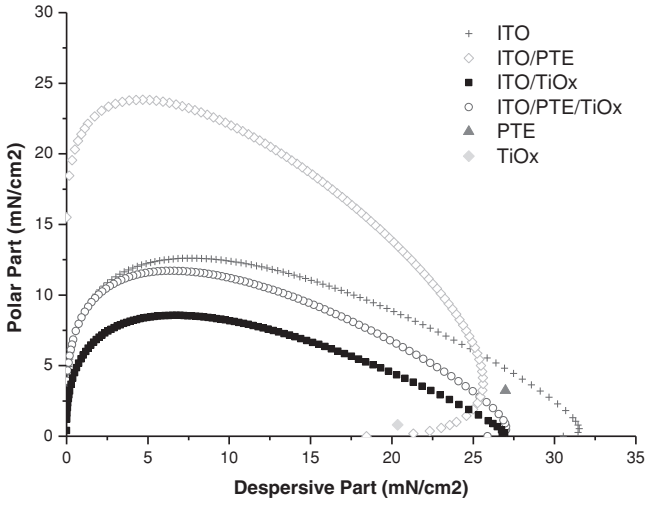


**Figure 7.** Wetting envelopes of ITO (cross), ITO/PTE/$TiO_x$ (circle), ITO/PTE (diamond), ITO/$TiO_x$ (square) and surface tensions of the liquids $TiO_x$ (filled diamond) and PTE (filled triangle).

## 3. Conclusions

In this paper, the effect of the cathode properties of solution processed organic and metal oxide interfacial layers for inverted OPV devices was investigated. For this purpose, a multi-layer electrode containing a PTE interfacial layer between the ITO and $TiO_x$ layers (ITO/PTE/$TiO_x$) was studied in comparison with an ITO/$TiO_x$ electrode. Surface properties of the different electrodes and sub structures were studied by XPS and UPS measurements, scanning electron microscopy and contact angle measurements. The XPS and UPS studies ruled out any chemical interaction between the $TiO_x$ and PTE layers, as well as any significant effect on the $TiO_x$ work function due to the PTE interfacial layer. The similar work functions are due to opposing interfacial dipoles observed. SEM measurements showed that incorporation of the PTE influences the surface

topography of the $TiO_x$ layer and the presence of gaps on the PTE surface. The incorporated PTE interfacial layer between ITO/$TiO_x$ improves the dispersion of the $TiO_x$ precursor solution as demonstrated through the reported contact angle measurements and thus $TiO_x$ becomes more hydrophilic when it is coated on top of PTE instead of ITO. Corresponding inverted OPV devices with ITO/PTE/$TiO_x$ bottom electrode showed improved electron selectivity compared to those on ITO/$TiO_x$ as reflected to their fill factors and PCE values.

We have shown that the incorporation of PTE interfacial layer between ITO/TiOx does not modify the energy levels but clearly affects the morphology, wetting properties and hydrophilicity of the TiOx. The above parameters improved electron selectivity of ITO/PTE/$TiO_x$ bottom electrode. The experimental results provide indications that the PTE interfacial layer between ITO/TiOx improved the functionality of the $TiO_x$ and enhanced vertical phase segregation of the P3HT:PCBM active layer within the inverted OPV structure increasing device performance. To conclude, we have shown that stacking solution-processed insulating polymer and metal oxide interfacial layers can be used as a method to control interfacial properties of inverted OPVs. We believe that the approach followed in this paper can also be used in other organic electronic applications using metal oxide based buffer layers.

## 4. Experimental Section

The photo-active layer of the devices is a blend of P3HT:PCBM in chlorobenzene, sandwiched between the two extracting electrodes. The current density-voltage (J–V) characteristics were measured with a Keithley source measurement unit (SMU 2420). For illumination a calibrated Newport Solar simulator was used providing an AM 1.5 G spectrum at 100 mW/cm$^2$. The Newport solar simulator is equipped with a metal halogen lamp. The device architectures studied are summarized as follows. The EQE measurements were carried out on a setup comprising a Xe lamp, a monochromator, a current-voltage preamplifier, and a lock-in amplifier. IQE curves were extracted by the division of the EQE for each device by the active layer absorption. The control devices using $TiO_x$ as an electron selective interfacial layer (ITO/$TiO_x$/P3HT:PCBM/PEDOT:PSS/Ag) are compared with devices with the PTE [$C_{13}H_{27}(OCH_2CH_2)_{12}OH$, Aldrich] interfacial layer inserted between the ITO and the $TiO_x$ electron selective contact (ITO/PTE/$TiO_x$/P3HT:PCBM/PEDOT:PSS/Ag). The PTE interfacial layer (0.1% in water) was doctor-bladed on ITO and estimated to be below 10 nm using a Dektak 150 profilometer. The $TiO_x$ precursor [tetra-n-butyl titanate, DuPont] was doctor-bladed on top of pre-sputtered ITO substrates (or on top of PTE) and annealed at 140 °C for 30 min in ambient conditions resulting to a layer thickness was found to be 40 nm. The active layer was doctor-bladed on top of $TiO_x$, resulting in a layer thickness of 230 nm. PEDOT:PSS [clevios PH, H.C. Starck] was doctor-bladed on top of the active layer. A fluorosurfactant [Zonyl FS 300, Aldrich] was used to improve the conductivity and adhesion properties of PEDOT:PSS. The devices were annealed inside a glovebox and after that a silver layer with a thickness of 100 nm was evaporated on top of PEDOT:PSS.

XPS measurements were carried out in a Specs/MAX 200 Ultra-high Vacuum (UHV) system. The specimens, prepared ex-situ, were introduced into the UHV chamber exactly as received and were mounted on an electrically grounded aluminum plate holder. The XPS measurements were carried out at room temperature under UHV in the low $10^{-9}$ mbar range using unmonochromatized $MgK_a$ radiation at 1253.6 eV and a constant pass energy of 48 eV for the EA200 analyzer, giving full width at half maximum (FWHM) of 1.2 eV for the Au $4f_{7/2}$. The analyzed area was an approximately $4 \times 7$ mm$^2$ rectangle positioned near the geometric center of each sample. The relative sensitivity factors (RSF) used for quantitative analysis were adapted to the MAX200 spectrometer operating conditions from the empirical RSF collection of Wagner et al.,[30] after correcting for the EA200 analyser transmission characteristics relative to those of Wagner's analyser.

For the UPS measurements a SPECS UV lamp was used with an analyzer resolution of 0.16 eV as determined from the width of the Au Fermi edge in a clean Au foil. A negative bias of 12.30 V was applied to the sample during UPS measurements in order to separate sample and analyzer high binding energy cut-offs and estimate the absolute work function from the UV photoemission spectra. The binding energy scale was referenced to the Au Fermi edge position and is valid for any grounded, conductive sample. It should be noted that, for all samples grounding was achieved via the conductive ITO layer.

XPS and UPS studies were performed for the following structures: a) ITO, b) ITO/$TiO_x$ c) ITO/PTE/$TiO_x$ and d) ITO/PTE. The ITO sample was used as a reference in all cases. The XPS wide scan spectra of the reference sample show that In, O, Sn are present on the surface. It is expected that the surface of any specimen analyzed by XPS in an UHV chamber will be covered by a ubiquitous surface contamination layer (typically ~0.8 nm thick and consisting primarily of hydrocarbons), due to sample exposure to the atmosphere. The actual thickness of the contamination layer (for carefully handled specimens) might depend on the underlying surface chemical composition. Surface evaluations of a) ITO/$TiO_x$ and b) ITO/PTE/$TiO_x$ were performed using Quanta 200 Scanning Electron Microscope (SEM) (FEI, Hillsboro, Oregon, USA) equipped with Energy Dispersive X-ray Spectroscopy (EDS).

Contact angle measurements were performed using a KRUSS drop shape analysis system in a cleanroom environment. The cleanroom environment does not prevent adventitious hydrocarbons which can influence the contact angle measurements, but we assume that if there is any contamination it is the same for all samples and therefore it will not affect the comparative hydrophilicity of the various measurements. A drop of water was deposited on each substrate measured and, with the assistance of an illuminated high speed camera, the angle between the surface and the water drop was measured. The value of the water contact angle was calculated by the EasyDrop software, using the sessile drop method.[31] For the surface energy measurements, the contact angle of known surface tension liquids was measured. Also, the polar and dispersive parts of the surface tension of each of the materials were calculated via pendant drop method and contact angle measurements on a standard Teflon surface. Based on these results, the software derived the polar and dispersive parts of the surface energy of the solids and hence the wetting envelopes. Wetting envelopes are closed curves that are obtained when the polar fraction of a solid is plotted against the disperse part.[32] With the help of the wetting envelope and knowledge of the polar and disperse parts of the SFE of a solid it is possible to predict whether a particular liquid whose surface tension components are also known will wet the surface completely. All liquids whose data lie within this enclosed area will wet the corresponding solid.

## Acknowledgements

This work was co-funded by the European Regional Development Fund and the Republic of Cyprus through the Research Promotion Foundation (Strategic Infrastructure Project NEA ΥΠΟΔΟΜΗ/ΣΤΡΑΤΗ/0308/06). AS whould like to thank K. Kapnisis for his assistance on the SEM measurements.

Received: April 3, 2012
Revised: September 4, 2012
Published online: November 2, 2012

[1] M. A. Green, K. Emery, Y. Hishikawa, W. Warta, *Prog. Photovolt: Res. Appl.* **2012**, *20*, 12.
[2] F. C. Krebs, *Sol. Energy Mat. Sol. C.* **2009**, *93*, 394.

[3] D. S. Hecht, L. Hu, G. Irvin, *Adv. Mater.* **2011**, *23*, 1482.
[4] N. Espinosa, M. Hosel, D. Angmob, F. C. Krebs, *Environm. Sci.* **2012**, *5*, 5117.
[5] J. A. Hauch, P. Schilinski, S. A. Choulis, R. Childers, M. Biele, C. J. Brabec, *Sol. Energy Mat. Sol. C.* **2008**, *92*, 727.
[6] C. H. Peters, I. T. Sachs-Quitana, J. P. Kastrop, S. Beaupre, M. Leclerc, M. D. McGehee, *Adv. Energy Mat.* **2011**, *20*, 1.
[7] C. N. Hoth, S. A. Choulis, P. Schilinsky, C. J. Brabec, *Adv. Mater.* **2007**, *19*, 3973.
[8] C. N. Hoth, P. Schilinsky, S. A. Choulis, C. J. Brabec, *Nano Lett.* **2008**, *8*, 2806.
[9] C. N. Hoth, R. Steim, P. Schilinsky, S. A. Choulis, S. F. Tedde, O. Hayden, C. J. Brabec, *Org. Electron.* **2009**, *10*, 587.
[10] M. Neophytou, W. Cambarau, F. Hermerschmidt, C. Waldauf, C. Christodoulou, R. Pacios, S. A. Choulis, *Microelectron. Eng.* **2012**, *95*, 102.
[11] M. Voigt, R. D. I. Mackenzie, C. P. Yau, P. Atienzar, J. Dane, P. E. Keivanides, D. D. C. Bradley, J. Nelson, *Sol. Energ. Mat. Sol. C.* **2011**, *95*, 731.
[12] M. Glatthaar, M. Niggemann, B. Zimmermann, P. Lewer, M. Riede, A. Hinsch, J. Luther, *Thin Solid Films* **2005**, *491*, 298.
[13] H. Oh, J. Krantz, I. Litzov, T. Stubhan, L. Pinna, C. J. Brabec, *Sol. Energy Mat. Sol. C.* **2011**, *95*, 2194.
[14] C. Waldauf, M. Morana, P. Denk, P. Schilinsky, K. Coakley, S. A. Choulis, C. J. Brabec, *Appl. Phys. Lett.* **2006**, *89*, 233517.
[15] H. Liao, L. Chen, Z. Xu, G. Li, Y. Yang, *Appl. Phys. Lett.* **2008**, *92*, 173303.
[16] M. Campoy-Quiles, T. Ferenczi, T. Agostinelli, P. G. Etchegoin, Y. Kim, T. D. Anthopoulos, P. N. Stavrinou, D. D. C. Bradley, J. Nelson, *Nat. Mater.* **2008**, *7*, 158–164.
[17] J. Nelson, *Mater. Today* **2011**, *14*, 462–470.
[18] S. H. Park, A. Roy, S. Beaupre, S. Cho, N. Coates, J. S. Moon, D. Moses, M. Leclerc, K. Lee, A. J. Heeger, *Nat. Photon.* **2009**, *3*, 297.
[19] C. E. Small, S. Chen, J. Subbiah, C. M. Amb, S. W. Tsang, T. H. Lai, J. R. Reynolds, F. So, *Nat. Photon.* **2012**, *6*, 115.
[20] Z. He, C. Zhong, S. Su, M. Xu, H. Wu, Y. Cao, *Nat. Photon.* **2012**, *6*, 591.
[21] X. Wang, T. Ishwara, W. Gong, M. Campoy-Quiles, J. Nelson, D. D. C. Bradley, *Adv. Funct. Mater.* **2012**, *10*, 1.
[22] R. Steim, S. A. Choulis, P. Schilinsky, C. J. Brabec, *Appl. Phys. Lett.* **2008**, *92*, 093303.
[23] M. V. Kuznetsov, J. F. Zhuravlev, V. A. Gubanov, *J. Electron. Spectrosc.* **1992**, *58*, 169.
[24] M. C. Biesinger, L. W. M. Lau, A. R. Gerson, R. St. C. Smart, *Appl. Surf. Sci.* **2010**, *257*, 887.
[25] S. Guttmann, M. A. Wolak, M. Conrad, M. M. Beerbom, R. Schlaf, *J. Appl. Phys.* **2011**, *109*, 113719.
[26] Y. Sahin, S. Alem, R. Bettignies, J. M. Nunzi, *Thin Solid films* **2005**, *476*, 340.
[27] T. Kuwabara, H. Sugiyama, T. Yamagushi, K. Takahashi, *Thin Solid Films* **2009**, *517*, 3766.
[28] S. Khodabakhsh, B. M. Sanderson, J. Nelson, T. S. Jones, *Adv. Funct. Mater.* **2006**, *16*, 95.
[29] Z. Xu, L. M. Chen, G. Yang, C. H. Huang, J. Hou, Y. Wu, G. Li, C. S. Hsu, Y. Yang *Adv. Funct. Mater.* **2009**, *19*, 1227–1234.
[30] C. D. Wagner, L. E. Davis, M. V. Zeller, J. A. Taylor, R. H. Raymond, L. H. Gale, *Surf. Interface Anal.* **1981**, *3*, 211.
[31] D. Y. Kwok, A. W. Neumann, *Adv. Colloid Interface* **1999**, *81*, 167.
[32] D. Janssen, R. De Palma, S. Verlaak, P. Heremans, W. Dehaen, *Thin Solid films* **2006**, *515*, 1433–1438.